# Flow past rectangular cylinders: receptivity to transverse forcing

## By B. T. TAN, M. C. THOMPSON and K. HOURIGAN

Fluids Laboratory for Aeronautical and Industrial Research (FLAIR), Department of Mechanical Engineering, PO Box 31, Monash University, Clayton, Victoria 3800, Australia

The flow at low Reynolds number around rectangular cylinders of varying chord-to-thickness ratios under transverse periodic forcing is studied numerically. Although of relatively low amplitude, the forcing locks the shedding from both the leading and trailing edges to the applied frequency. The base suction, and the lift and the drag on the cylinders are found to be complex functions of the forcing frequency. At low Reynolds numbers and without applied forcing, the flow is controlled by a global instability with the leading- and trailing-edge shedding locked; moreover, the reduced frequency of shedding varies in a stepwise manner with the chord-to-thickness ratio. This global instability is still evident in the flows under external forcing examined in this paper. While previous researchers have conjectured that the trailing-edge shedding plays a dominant role in the preferred frequency selection in the natural shedding case, the important role of trailing-edge shedding when the flow is forced is confirmed in the present study. In particular, the individual contributions from leading- and trailing-edge vortices on the perturbation to the leading-edge shear layer are examined. In addition, it is shown that the base suction is maximum when the forcing frequency is close to the global instability frequency observed in unforced flows, thereby strengthening the argument that the unforced, forced, and duct resonant cases are strongly influenced by the same global instability. The variations of the lift, drag and formation length with chord-to-thickness ratio are quantified.

## 1. Introduction

Strong emphasis is found in the literature on the flow around just one example of the elliptic cylinder, namely the circular cylinder (see review by Williamson 1996). The Universal Strouhal number relationship, proposed by Roshko (1954, 1995) to be independent of body shape, suggested that the circular cylinder is a generic shape for all two-dimensional bluff bodies. This has been supported by measurements for a large range of body shapes by Griffin (1981). However, recent investigations of the flow at relatively low Reynolds numbers around elliptic cylinders of different eccentricities suggest that the circular cylinder does not adequately represent the full richness of the two-dimensional wake structure of elliptic cylinders (Johnson, Thompson & Hourigan 2001). Furthermore, there is a complexity of flow structure and vortex interactions in flow around rectangular cylinders that does not exist for the 'generic' circular cylinder geometry (Hourigan, Thompson & Tan 2001). As its chord-to-thickness ratio is varied from zero to infinity, the rectangular cylinder also encompasses the range of bluff bodies from a flat plate normal to the flow, the square cylinder, through to a flat plate parallel to the flow. Given the many examples of

rectangular cross-section that appear in practical flows, for example in flows around buildings and through cross-flow heat exchangers, a greater understanding is needed of their flow characteristics.

In this article we consider the boundary layer and wake response of flow past elongated two-dimensional cylinders of rectangular cross-section subject to transverse sinusoidal forcing. Even a small-amplitude forcing can result in significant changes to the flow characteristics (Welsh *et al.* 1990). This study focuses on two of the inherent receptivities/instabilities that exist in this flow and the interaction between them. The oncoming flow separates from the leading edge to form a separated shear layer. At the chord-to-thickness ratios considered, it reattaches along the surface of the cylinder forming discrete vortex structures that travel downstream and pass into the wake. At the trailing edge, the boundary layers from each side of the cylinder interact through a global instability leading to vortex shedding and the Bénard/von Kármán wake. Of primary interest to this research is the interaction between the absolute shedding instability at the trailing edge and the receptivity of the shear layer at the leading edge. The type of flow excitation studied here has been categorized as *extraneously induced excitation* (EIE); one of the three broad groupings defined by Naudascher & Rockwell (1994).

In the absence of any external disturbance, the leading-edge shear layer experiences a low-frequency flapping and shedding of large-scale vortices into the boundary layer is irregular (Cherry, Hiller & Latour 1984). A shorter reattachment bubble, stronger surface pressure fluctuations and more coherent large-scale structures have been observed when low-level transverse acoustic forcing is applied (Sigurdson 1995). Although the shear layer amplifies a broad band of frequencies, it is more responsive to frequencies associated with the Kelvin–Helmholtz instability and large-scale shedding (Sigurdson 1995; Wu & Soria 1992; Soria, Sheridan & Wu 1993).

The response of the absolute instability near the trailing edge of blunt cylinders to external excitation has been shown to be similar to that of short bluff bodies in experiments by Lofty & Rockwell (1993). The flows around short bluff bodies such as circular and square-sectioned cylinders with excitation have been well-studied and are reviewed by Bearman (1984). In line with the theoretical predictions of absolute instability, the shedding only locks on to the low-amplitude applied forcing in a narrow frequency range around the natural shedding frequency, which is known as the resonant point. Stronger base suction (Stansby 1976; Bearman & Davies 1977; Blackburn & Henderson 1996) and hence drag, and larger fluctuating lift forces (Staubli 1983; Bearman & Obasaju 1982), due to an increased spanwise correlation and reduced vortex formation lengths have been observed within this range of capture. In some cases, a phase shift of $\pi$ is observed between the excitation and the shedding at some point in this range. This lock-in range has been shown to grow with larger forcing levels with a quasi-periodic state observed just outside this range (Karniadakis & Triantafyllou 1989). At forcing frequencies well above the lock-in range, some experiments have observed the mean base suction to fall below that of the unforced case (Bearman & Obasaju 1982; Ongoren & Rockwell 1988).

In the absence of any external forcing, the non-dimensional shedding frequency or Strouhal number ($St_c = fc/U_\infty$, where $f$ is the measured wake frequency, $c$ is the chord or cylinder length, and $U_\infty$ is the upstream velocity) for the flow around a long rectangular cylinder displays a stepwise increase with increasing chord-to-thickness ratio $c/t$ (Nakamura, Ohya & Tsuruta 1991), where $t$ is the cylinder thickness. Note that the Strouhal number based on cylinder thickness $St_t$ is also relevant to the current study; in addition, there are the corresponding Strouhal numbers based on the forcing

frequency for the forced flows, $St_{fc}$ and $St_{ft}$, respectively. Each step corresponds to a different shedding mode, which is characterized by a different number of vortex pairs ($n$) between the leading and trailing edge. Thus, $n$ represents the number of vortices along the top or bottom surface of the cylinder. This stepping behaviour relies on a feedback mechanism as follows. Weak pressure pulses are generated from vortices shed from the leading edge as they pass the trailing edge, locking subsequent leading-edge shedding. This mechanism has been called the *impinging leading-edge vortex instability* (ILEV) by Naudascher & Wang (1993), and Naudascher & Rockwell (1994). Numerical simulations by Hourigan *et al.* (2001) showed the presence of strong shedding from the trailing edge resulting from the boundary layer rolling up as it convects past the trailing edge. That study suggested the ILEV mechanism needs to be extended to include the pressure fluctuations from the direct shedding at the trailing edge. Thus, it is suggested that the feedback mechanism should include the interaction of trailing-edge vortices (TEVs) as well ILEVs as was originally proposed. Since this trailing-edge shedding operates only over a narrow frequency range, unlike the leading-edge shear layer shedding, it can exert a controlling influence on the frequency selection and, in particular, the range of chord-to-thickness ratios that lock on to a particular shedding mode, i.e. the size of the step. Importantly, in this paper a comparison is made of the influence of ILEVs and TEVs on the leading-edge shear layer and hence of the controlling feedback mechanism. In either case, as the feedback mechanism is relatively weak, the flow gradually loses synchronization with increasing Reynolds number and chord-to-thickness ratio so that for $Re > 2000$ and $c/t > 12$, there appears to be no observable effect of the feedback loop (Nakamura *et al.* 1991).

With the aid of an external influence, the synchronization between the leading- and trailing-edge shedding can be re-established. The flow appears to be receptive to approximately the same Strouhal numbers as in the earlier case (i.e. for natural shedding at lower Reynolds numbers). This has been shown in experiments in two different ways. First, when the flow is subjected to transverse acoustic forcing (Parker & Welsh 1983; Mills *et al.* 1995; Mills, Sheridan & Hourigan 2002; Mills 1998), and secondly, where the cylinder is placed in a duct and the resonant cross-stream acoustic mode is excited (Stokes & Welsh 1986). In the first case, the experiments by Parker & Welsh (1983) showed that the acoustic forcing locks the shedding from the leading edge and these vortices travel along the cylinder and into the wake while maintaining the same frequency. Those experiments also show a greater curvature of the leading-edge shear layer resulting in a shorter reattachment length and stronger surface suction with the applied forcing. Base pressure measurements were recorded for a cylinder in an open jet wind tunnel following that study (Mills *et al.* 1995, 2002; Mills 1998). When the forcing Strouhal number ($St_{fc}$) that resulted in the strongest mean base suction for each chord-to-thickness ratio is considered, it also shows a stepwise increase with chord-to-thickness ratio similar to the natural shedding case. For the second case, when the cylinder is placed centrally in a duct, the duct resonance frequencies that lock the flow and sustain the resonance also showed a similar stepping (Stokes & Welsh 1986). In both these cases, the weak pressure pulse in the feedback loop is replaced by an external influence, either directly by external forcing, or indirectly by a self-excited resonant acoustic field. In effect, these experiments show that the underlying mechanism of the ILEV/TEVS instability can still exert a strong influence even at higher Reynolds numbers.

A numerical study of flow around long rectangular cylinders under low-amplitude transverse oscillatory forcing is presented in this paper. This complements and extends

the experimental studies of Mills (1998), and Mills *et al.* (2002), especially by providing and interpreting significantly more quantitative measurements not available from the experiments. For the amplitudes considered, the cross-stream forcing is effectively equivalent to oscillating the cylinder. This has been verified by numerical experiments. In addition to the experimental results of Mills (1998), comparisons are also made with results of an investigation into the unforced or natural flow case presented by Hourigan *et al.* (2001). The range of chord-to-thickness ratios studied is $3 < c/t < 16$ for the natural shedding case, and $6 < c/t < 16$ for the forced shedding case. Surface pressure and force coefficients are used to gauge the response of the system to the applied forcing. Flow visualization is then used to analyse other important features such as shedding modes and phasing. The convective velocity of the vortices and the vortex formation length are also used to relate the flow field to the overall response. Finally, the evidence supporting the more substantial role of the trailing-edge vortices in the feedback mechanism is presented.

## 2. Numerical method

The spectral-element method is used in this study, as described in Thompson, Hourigan & Sheridan (1996), and Hourigan *et al.* (2001). A general description of the method is given in Sherwin & Karnidakis (2001). The method and implementation have been described in detail and validated for previous related studies (Thompson *et al.* 1996; Tan, Thompson & Hourigan 1998; Sheard, Thompson & Hourigan 2003), so only the necessary details are presented here. The method is second-order in time and obtains spectral convergence for smooth problems. The effect on the flow of the sharp corners of the cylinder is to induce minor oscillations in the vorticity field in the macro-elements immediately adjacent to the corners. However, the effect remains localized to these elements and does not cause significant degradation of the solution field elsewhere. This is unlike the situation for a global method, where the oscillations can significantly contaminate the solution throughout the domain. To verify this point, some simulations were repeated for $c/t = 7$ using a second-order finite-volume method with a very fine mesh in the neighbourhood of the cylinder. The predicted Strouhal number and base pressure coefficient were within 3% of the values predicted using the spectral-element method.

The conditions applied at the boundaries of the computational domain are, in the case of no forcing: (i) no slip on the cylinder; (ii) zero normal velocity derivative at the outflow boundary; and (iii) on the side and inflow boundary the velocity was taken as uniform in the horizontal direction. The global applied perturbation is a sinusoidally oscillating velocity component in the transverse direction added to the velocity at all free-stream boundaries, equivalent to adding an oscillatory component to the free-stream flow. This is applied once the flow has reached an asymptotic state in the absence of forcing and the forced flow is then simulated until it reaches a new typically periodic asymptotic state. A typical computational mesh displaying the macro-elements employed for the rectangular cylinder with $c/t = 10$ is shown in figure 1. Only the macro-elements are shown; each element is further subdivided into $N_x \times N_y$ nodes. Typically $N_x = N_y = 7$ or 9.

### 2.1. *Selection of Reynolds number*

The choice of Reynolds number for the simulations is a compromise. A large parameter space is considered, with variations in chord-to-thickness ratio and forcing frequency, and to a lesser extent, forcing amplitude. This scope effectively rules out
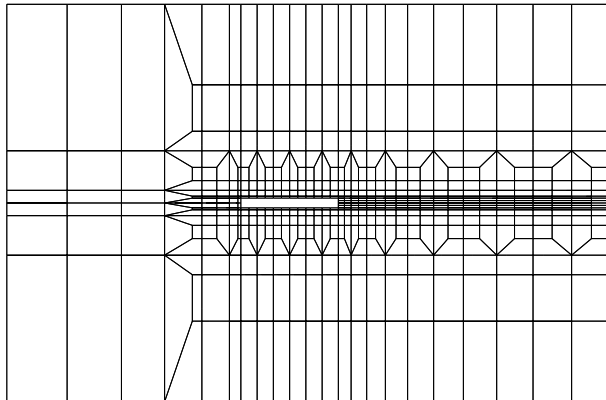
FIGURE 1. A typical computational mesh showing the macro elements used in simulations
($c/t = 10$).

expensive three-dimensional large-eddy simulations that could perhaps match the
typical Reynolds numbers used in the experiments of between $10^3$ and $10^4$.

Three-dimensional direct numerical simulations (Tan 2000) show that the unforced
flow becomes three-dimensional at approximately $Re = 350$–400, with some variation
with chord-to-thickness ratio. This result is broadly consistent with Sasaki & Kiya
(1991), who found that for very high chord-to-thickness ratio cylinders, the onset of
three-dimensional flow occurred at $Re \approx 320$. In both cases, the three-dimensionality
develops from the leading-edge separation bubble. Further numerical simulations
indicate that the introduction of transverse forcing raises that transition Reynolds
number to above $Re = 600$ (Tan 2000). The water tunnel experiments of Hourigan
*et al.* (1993) show the forced flow is clearly three-dimensional at $Re = 1000$, with the
boundary layer and wake structures much more ordered than in the unforced case.
Given this background, a Reynolds number of 400 was chosen for this study and
two-dimensional simulations were used to predict the flow. This Reynolds number is
high enough for strong vortical structures to form from both the leading and trailing
edges of the cylinder and it is these structures that appear to govern the flow physics.
In addition, since the flow is forced, the effect of three-dimensionality and turbulence
is reduced. Indeed, the flow is two-dimensional at this Reynolds number. Hence this
two-dimensional modelling is expected to accurately reflect the behaviour at $Re = 400$.
In addition, a comparison of the numerical predictions with experimental results at
higher Reynolds numbers indicate that the trends in the force coefficients with forcing
frequency and chord-to-thickness ratio are in broad agreement with the experimental
trends, as is the observed Strouhal number stepping.

### 2.2. *Numerical resolution*

Simulations with different resolutions were performed to verify that the chosen
resolution was sufficient to accurately capture the flow behaviour. These were
performed with the same macro-element grid, but with different degree tensor-
product interpolating polynomials within macro-elements. Results were obtained
using $N_x \times N_y = 7 \times 7$ and $N_x \times N_y = 9 \times 9$ internal nodes per element. The timestep
was also decreased for the higher spatial resolution simulations because of the
Courant constraint: from $\Delta t = 0.007$ to $\Delta t = 0.004$. Comparison simulations were
performed for $c/t = 10$ and $St_{ft} = 0.14 - 0.18$ at 5 regular intervals. Within this range
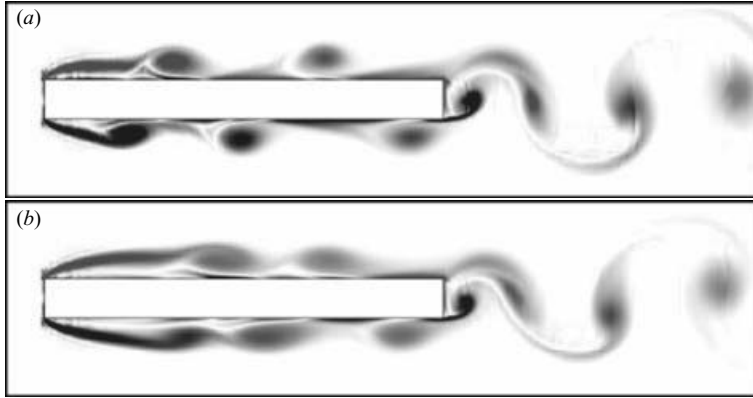of forcing, the mean base suction varied between $0.46 < c_p < 1.22$. Over this range,

FIGURE 2. Vorticity plots for flow around a cylinder with $c/t = 10$. (*a*) Taken at 90° in the forcing cycle with $St_{ft} = 0.16$ and $v_{pert} = 2.5\%$. (*b*) No applied forcing and taken at approximately the same phase in the shedding cycle. Contouring level range is $\pm 0.2$ to $\pm 4$. This range is applicable to all subsequent vorticity plots. Vorticity has been non-dimensionalized by cylinder thickness and upstream speed.

the deviations from the predictions using the lower resolution were less than 2%. This was considered an acceptable tolerance and so the lower resolution of $N_x \times N_y = 7 \times 7$ was assumed to be sufficient for the bulk of the simulations.

## 3. Results

This section examines the influence of a small sinusoidal cross-flow oscillation on the flow around a long rectangular cylinder. Initially, the base pressure is used to indicate the response of the flow to the applied forcing and compared with experimental data. The overall force coefficients are presented next. This is followed by some flow visualization and further post-processing to aid in the interpretation of the predicted quantities.

Figure 2 shows shaded contours of vorticity for flow past a cylinder with $c/t = 10$ and $Re = 400$ for the cases with and without forcing, to illustrate the substantial effect of applied forcing. For the forced case, the plot is taken at 90° in the sinusoidal forcing cycle with perturbation amplitude $v_{pert} = 2.5\%$ and $St_{ft} = 0.16$. At this frequency, the strongest mean base suction is recorded in the lock-in range for this chord-to-thickness ratio and forcing amplitude. The vorticity plot in the natural shedding case is taken at a phase in the shedding cycle that approximately matches the forced case. There are several key differences compared with the natural shedding cases described by Hourigan *et al.* (2001). Starting from the leading edge, the shear layer reattaches earlier and more-compact vortices are shed. These vortices remain more compact while they convect toward the trailing edge and coalesce with the vortices shed from there. The vortices at the trailing edge are marginally more compact than those in the natural shedding case.

### 3.1. *Mean base pressure*

The flows for $6 \leqslant c/t \leqslant 16$ are simulated for a range of forcing frequencies at $Re = 400$ and $v_{pert} = 2.5\%$. Unless otherwise stated, these values are fixed for all following sections. A large lock-in range is observed for all the cylinders; the range varied from $St_{ft} = 0.13$ to 0.20 (highest frequency simulated) for the shortest cylinder ($c/t = 6$) to $0.09 \leqslant St_{ft} \leqslant 0.19$ for the longest cylinder ($c/t = 16$). The large lock-in range is possibly

a result of the large receptivity range of the leading-edge shear layer combined with the suppression of the narrow-band trailing-edge shedding through interference from passing leading-edge vortices. When the flow is locked, both the leading- and trailing-edge shedding locks on to the single forcing frequency.

The behaviour of the time-mean base pressure coefficient measured at the centre of the trailing face as a function of forcing frequency, both predicted by the simulations and measured experimentally by Mills (1998), and Mills *et al.* (2002), is shown in figure 3. Referring to the simulations, cylinders with a chord-to-thickness ratio of $c/t = 6$, 7, 10, 11, 15 and 16 show a single peak in the mean base suction equivalent to a local minimum in base pressure coefficient. These peaks are larger than for cylinders with chord-to-thickness ratios of $c/t = 8$, 9, 12, 13 and 14. For the second set, there are two less prominent peaks, and at times one of them is barely noticeable. For reasons that will become clear later, it is convenient to group local peaks in the mean base pressure into two categories. The main group or *primary* peaks consists of all cases that show only a single peak and the local peak associated with the lower forcing frequency in those cases with two local peaks. The remainder or *secondary* peaks consists of the local peak that occurs at the higher forcing frequency in those cases that display two local peaks.

There is a functional dependence of the frequency at which the mean base suction peaks on chord-to-thickness ratio for both groups. Consider the primary, i.e. dominant, peaks first. Beginning with $c/t = 6$, a local maximum base suction, or minimum base pressure coefficient, is recorded for $St_{ft} = 0.17$. As the chord-to-thickness ratio is increased to $c/t = 7$, the Strouhal number at which maximum base suction occurs drops to $St_{ft} = 0.16$, then $St_{ft} = 0.14$ for $c/t = 8$ and $St_{ft} = 0.12$ for $c/t = 9$, with the last two of smaller magnitude. There is a jump in frequency when increasing the chord-to-thickness ratio to $c/t = 10$ which shows only a single peak at $St_{ft} = 0.165$. Then with increasing chord-to-thickness ratio, this peak shifts to $St_{ft} = 0.155$ for $c/t = 11$, $St_{ft} = 0.14$ for $c/t = 12$, $St_{ft} = 0.13$ for $c/t = 13$ and $St_{ft} = 0.11$ for $c/t = 14$, with again the last two being of relatively lower amplitude. Similar to the trend starting at $c/t = 10$, there is a single larger peak at $St_{ft} = 0.155$ for $c/t = 15$ which then decreases to $St_{ft} = 0.145$ at $c/t = 16$. The same process also occurs for the secondary group of peaks. At $c/t = 8$, the peak is at $St_{ft} = 0.174$ and it reduces to $St_{ft} = 0.162$ when $c/t = 9$. The same trend again is seen for $c/t = 12$, 13 and 14 with peaks at $St_{ft} = 0.17$, 0.157 and 0.155 respectively.

Alongside each plot in figure 3 is an arrow showing the predicted mean base pressure coefficient when no forcing is applied. The natural shedding frequency for the simulated cases that lock on to a single frequency is also shown.

## 3.2. *Lift and drag forces*

In the previous sections, the focus was on the pressure at a single point on the cylinder. Here, the overall force coefficients are examined. The mean drag coefficient and the standard deviation of the lift coefficient, which quantifies the fluctuating lift force, are examined for a range of cylinder chords and forcing frequencies. Only the pressure forces are considered because the viscous forces are relatively small at these moderate Reynolds numbers. It is relatively simple to calculate the forces on a rectangular cylinder as only the leading and trailing faces contribute to drag and the top and bottom faces contribute to lift forces.

The mean drag coefficient and the fluctuating lift coefficient are plotted in figure 4 for $6 \leqslant c/t \leqslant 16$ for a range of forcing frequencies. As expected, the mean drag force coefficient closely mimics the mean base pressure coefficient. As the contribution from
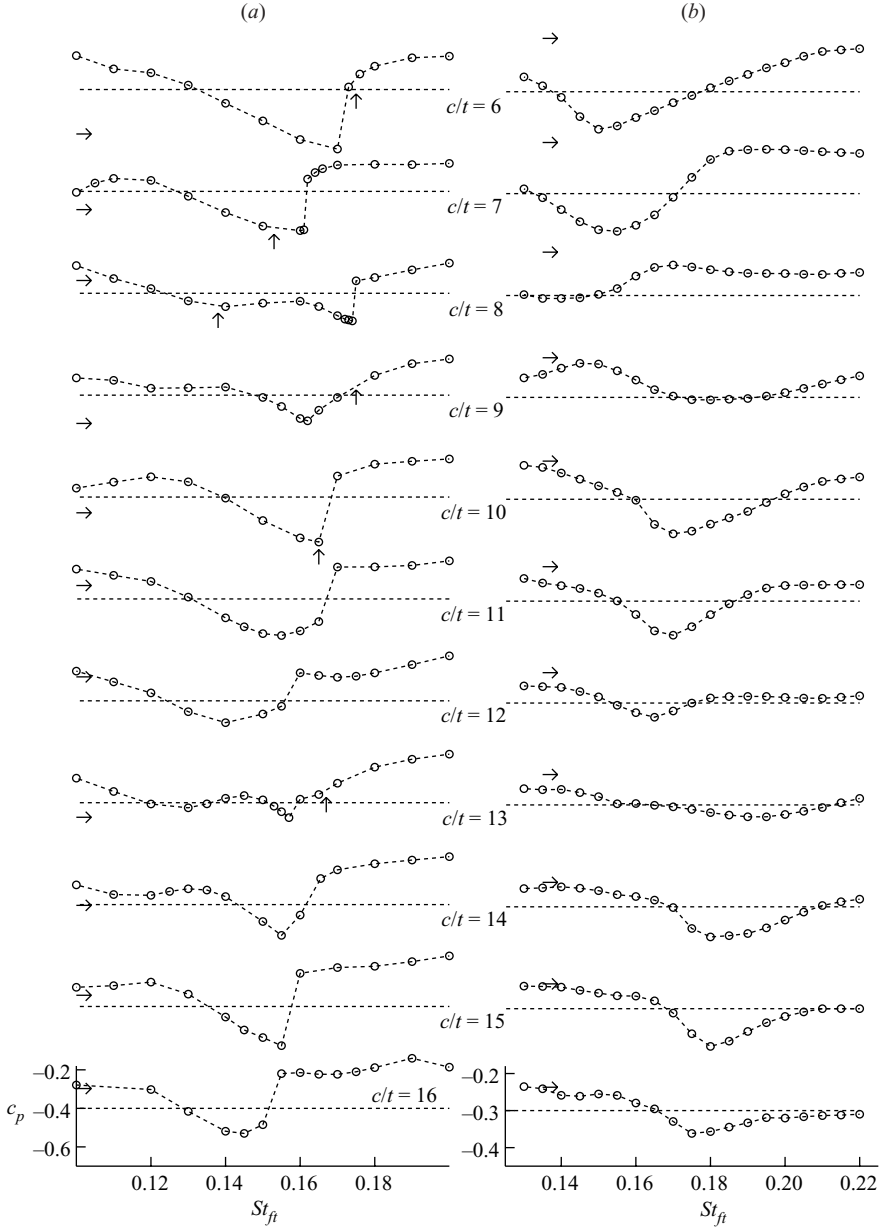
FIGURE 3. (*a*) Mean base pressure coefficient as a function of forcing frequency for cylinders in the range $6 \leqslant c/t \leqslant 16$ simulated at $Re = 400$ with a perturbation amplitude of $v_{pert} = 2.5\%$ (*b*) Experimental results recorded for $Re \approx 9000$ with forcing amplitude of 5% of the free-stream velocity measured at a different location. Horizontal arrows show the mean base suction for the unforced case. Vertical arrows show the natural shedding frequency for the unforced case.

the leading face is close to constant for all cases, the variation in mean drag force coefficient is chiefly a result of the trailing-face contribution (i.e. the mean frontal drag coefficient $\overline{c_d} = 0.774$–$0.851$ for $c/t = 10$ and $\overline{c_d} = 0.808$–$0.833$ for $c/t = 13$, for all the forcing frequencies simulated). The mean base pressure coefficient is strongly related to the pressure force acting on the back face of the cylinder. The dependence
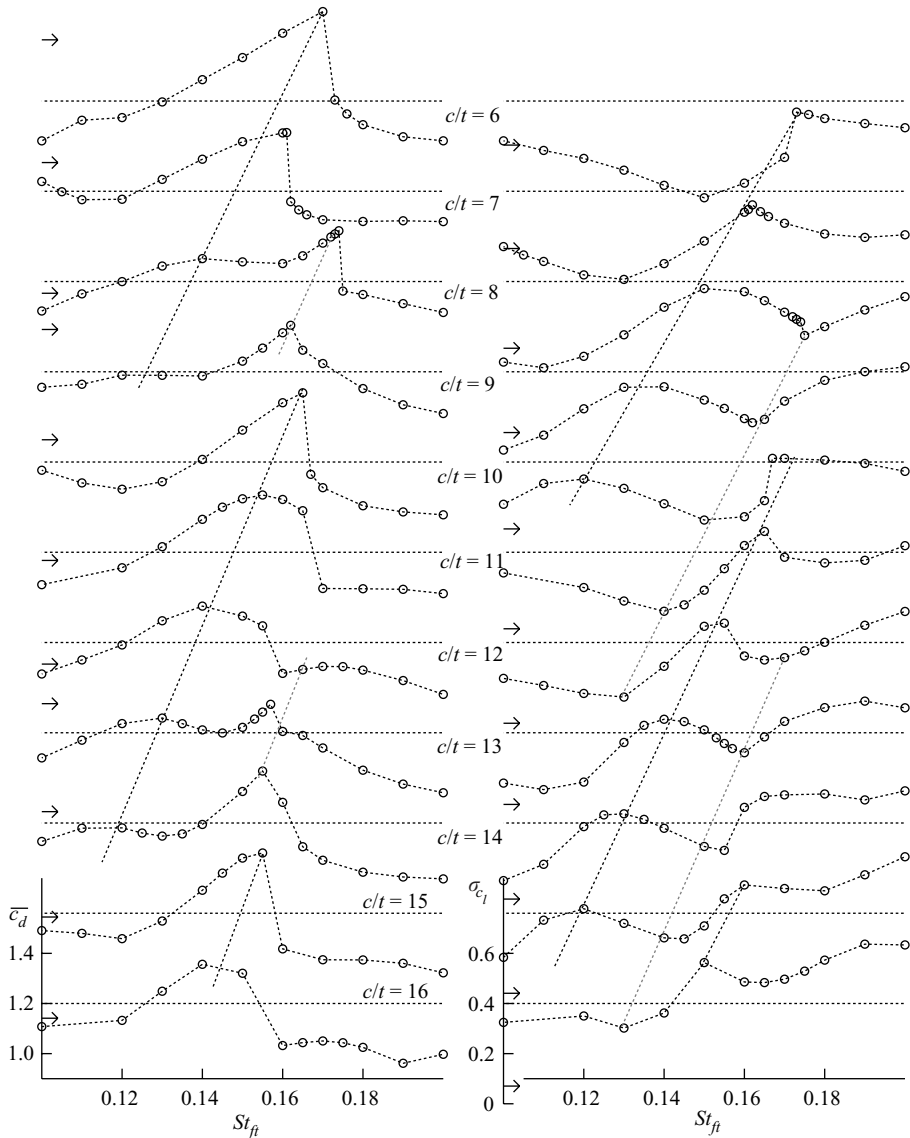
FIGURE 4. (*a*) Mean drag coefficient and (*b*) standard deviation of the lift coefficient as a function of forcing frequency for cylinders with $6 \leqslant c/t \leqslant 16$ at $Re = 400$ and $v_{pert} = 2.5\%$. The arrows on the left show the mean drag coefficient and the standard deviation of the drag coefficient when no forcing is applied. The dashed black lines approximately connect the *primary* peaks and the dashed grey lines connect the *secondary* peaks.

of the local maxima in mean drag coefficient as the chord-to-thickness ratio is varied is similar to that for the mean base suction. This is indicated by the two sets of dashed lines.

The plots of fluctuating lift force show some quantitative differences to the behaviour observed for the mean drag. Overall, there is a gradual rise in the fluctuating lift force with frequency. This is a result of the larger acceleration of the applied forcing field, especially near the cylinder. Compared with the mean drag or mean base pressure plots, the standard deviation in the lift coefficient shows a
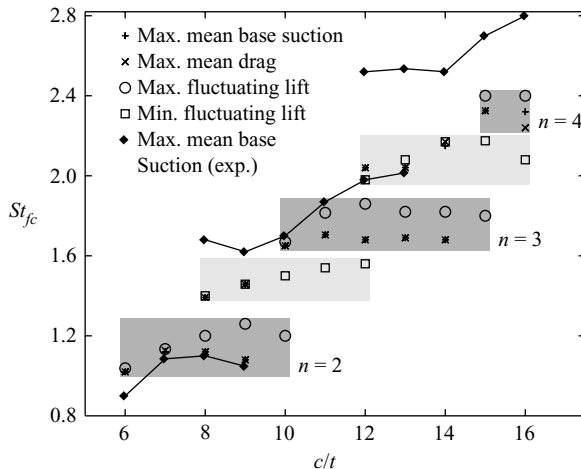
FIGURE 5. Strouhal number for the applied forcing frequency (non-dimensionalized with chord), $St_{fc}$, which results in a local peak in the mean base suction, mean drag and fluctuating lift as a function of the chord-to-thickness ratio for the present simulations. The local peaks in mean base suction from experiments by Mills (1998) and Mills *et al.* (2002) are also shown.

local maximum for cases associated with the primary peaks and a local minimum for cases associated with the secondary peaks. The black/grey dashed lines in figure 4 mark these trends.

### 3.3. *Frequency selection*

Using the data on the mean base pressure, and drag and fluctuating lift forces for various forcing frequencies and cylinder chords (figures 3 and 4), the Strouhal number based on chord of the forcing ($St_{fc}$) at which these local peaks occur is plotted in figure 5. The experimental measurements of mean base pressure from Mills (1998), and Mills *et al.* (2002) is also plotted. Note that the *primary* peaks, corresponding to local maxima in mean base suction, drag and fluctuating lift show a stepwise increase which is highlighted by the darker boxes. Each step corresponds to a particular shedding mode, *n*, which will be shown later in §3.4.3 to correspond to the number vortices formed along the cylinder. This stepwise trend is also seen in the experimental results. The intermediary steps corresponding to the *secondary* peaks, which also display a local maximum in mean base suction and drag but a local minimum in fluctuating lift are shown by the lighter boxes.

### 3.4. *Dynamics of the flow*

In this section, visualizations of the flow fields are used to relate the Strouhal number stepping to vortical flow structures. Previous studies have linked the phasing of vortical structures to the frequency selection (Hourigan *et al.* 1993; Mills 1998; Hourigan *et al.* 2001; Mills *et al.* 2002). To address this issue through the numerical simulations, the phasing at the leading edge relative to the forcing, the convective velocity of the vortices along the cylinder, and finally the resulting phase of the shedding relative to the forcing, are examined, providing strong support for the vortex interaction hypothesis. The link between the variation in magnitude of the peak base suction for different chord-to-thickness ratios and the trailing-edge shedding is shown by measuring the vortex formation length past the trailing edge.
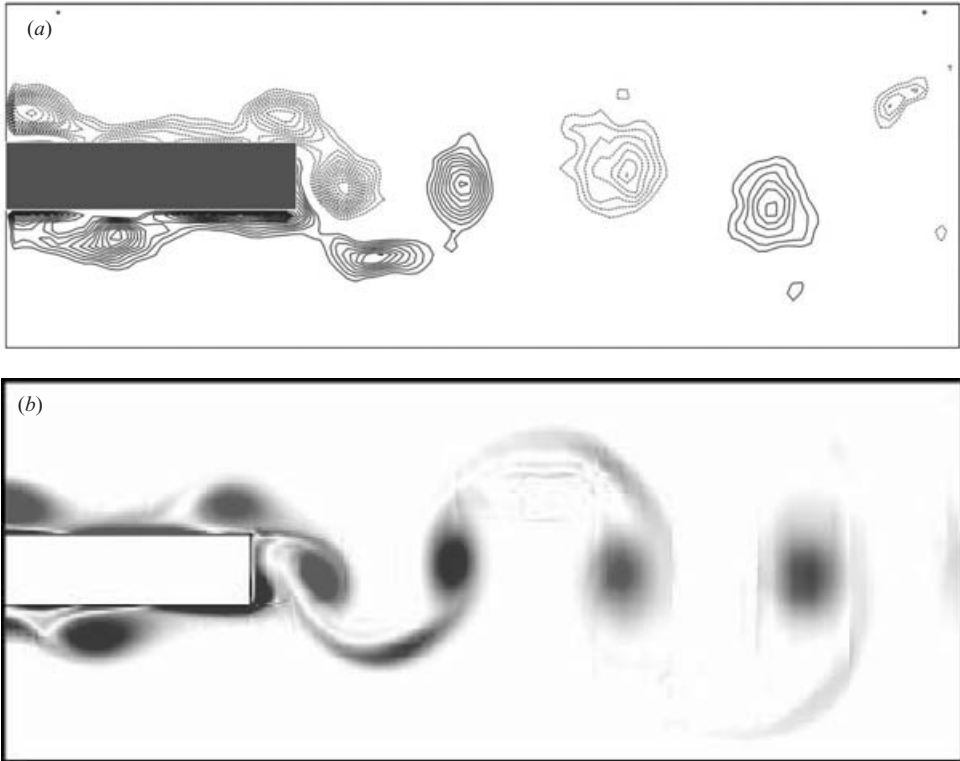
FIGURE 6. Comparison between the wake (*a*) observed in an experiment (Mills 1998) and (*b*) predicted numerically for flow over a cylinder with $c/t = 6$. The experimental plot is derived from PIV data and forced at $St_{ft} = 0.192$. The simulation is forced at $St_{ft} = 0.17$. Both plots are taken at 0° in the forcing cycle.

At this stage, numerical and experimental flow visualizations are compared. Figure 6 shows the wake structure for $c/t = 6$ taken at 0° in the forcing cycle. Figure 6(*a*) (Mills 1998; Mills *et al.* 2002) is obtained from PIV measurements in a water tunnel at $Re = 900$. The forcing frequency in that case is $St_{ft} = 0.192$, corresponding to the natural shedding frequency. The forcing frequency in the simulation at $Re = 400$ is $St_{ft} = 0.17$, which results in the maximum base suction and is also approximately the natural shedding frequency. The visualizations are strikingly similar in terms of overall positions of the leading and trailing vortices. This supports the relevance of the current numerical results to the higher Reynolds number three-dimensional flows used in the experiments. The slight difference in Strouhal numbers is a Reynolds number effect probably due to slight differences in the mean convection velocity of leading-edge vortices along the cylinder.

### 3.4.1. *Phasing of the leading-edge shedding*

In the cases where the flow is locked to the forcing, the leading-edge shedding is phase locked. The phase of shedding relative to the forcing also appears to be constant for all chord-to-thickness ratios and forcing frequencies investigated. To show this, three extreme cases are chosen: a shorter cylinder at a lower frequency ($c/t = 8$ and $St_{ft} = 0.11$); a longer cylinder at an intermediate frequency ($c/t = 16$ and $St_{ft} = 0.15$); and an intermediate cylinder at a higher forcing frequency ($c/t = 10$ and

$St_{ft} = 0.11, c/t = 8$ $St_{ft} = 0.15, c/t = 16$ $St_{ft} = 0.20, c/t = 10$
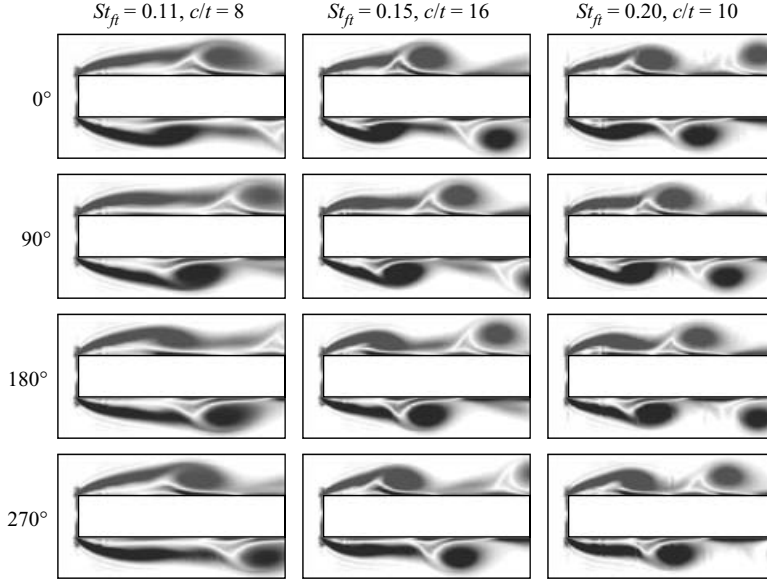


FIGURE 7. Vorticity plots of the leading-edge shedding at $Re = 400$ and $v_{pert} = 2.5\%$. Vorticity plots taken at 0°, 90°, 180° and 270° in the forcing cycle for cylinders with $c/t = 8$, 16 and 10 at applied forcing frequencies of $St_{ft} = 0.11$, 0.15 and 0.20 respectively.

$St_{ft} = 0.20$). Figure 7 shows the leading-edge shedding of these three cases at 0°, 90°, 180° and 270° in the forcing cycle. When the forcing frequency is increased, the shear layer rolls up closer to the leading edge but the phase of shedding relative to the forcing in each case is approximately the same. Further flow visualizations in § 3.4.3 (figures 9–11) also confirm that the phase of the leading-edge shedding relative to the forcing remains fixed in all cases.

### 3.4.2. *The convective velocity*

The streamwise component of velocity of the vortices as they convect along the cylinder is the focus of this section. This feature is crucial because it governs the time taken for a leading-edge vortex to pass the trailing edge, thereby affecting the phasing there. The following cases are investigated: (i) different cylinder lengths for the natural shedding case; (ii) different forcing frequencies for a fixed cylinder length; and (iii) different cylinder lengths for a constant forcing frequency.

To evaluate the convective velocity of the vortices, their locations are determined at regular time intervals. The local maximum in vorticity is used to define the location of a vortex. This is found by the Newton–Raphson method using polynomial interpolation within elements matching the order of the spectral-element scheme. The velocity is evaluated using central differencing between these locations. The sampling is performed every 0.21 time units over 8 to 10 time units, which is more than one shedding period. The convective velocities of the vortices on both sides of the cylinder are then calculated.

Figure 8 shows the convective velocity of the vortices as they traverse the length of the cylinder for the three classes studied. Figure 8(*a*) shows the convective velocity for flow over cylinders for $c/t = 6$, 8, 10 and 13 with no external forcing. Shown in figure 8(*b*) is the convective velocity for $c/t = 8$ at forcing frequencies of $St_{ft} = 0.11$,
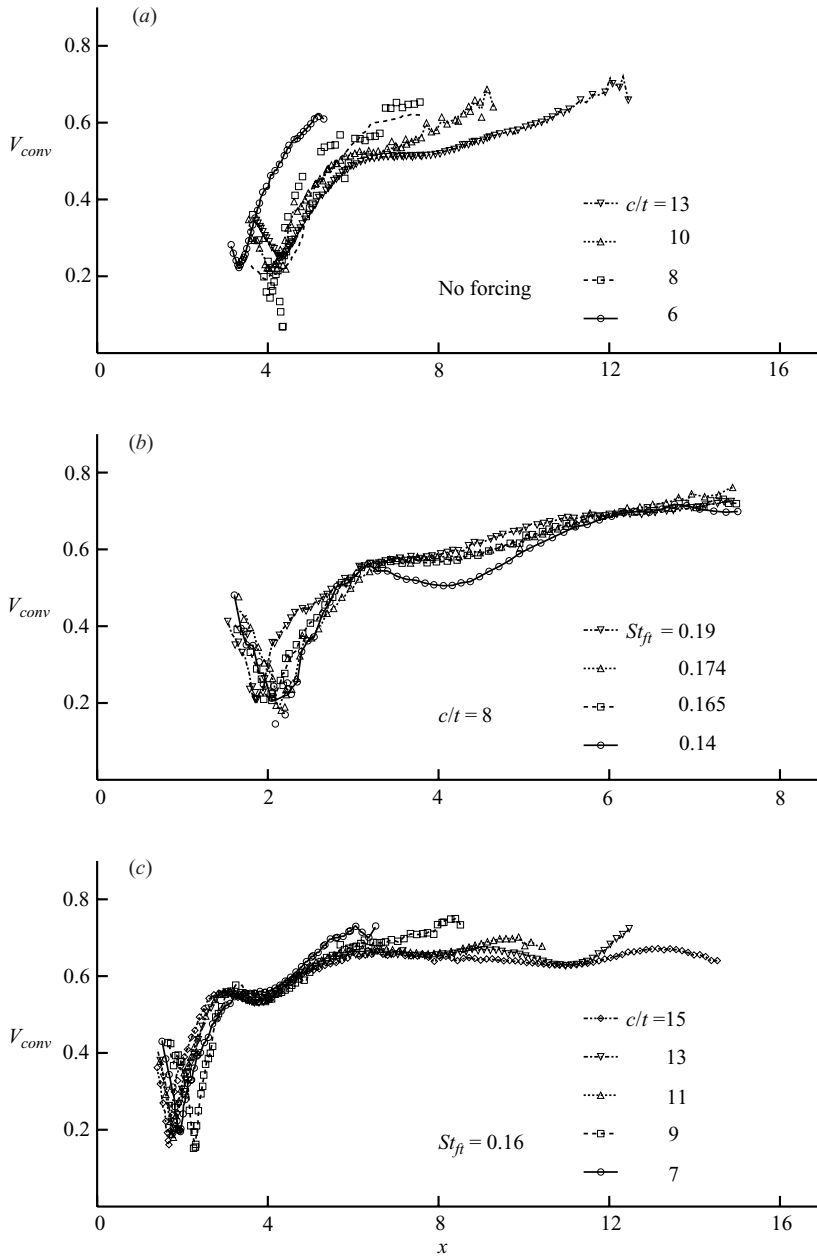
FIGURE 8. Streamwise component of the convective velocity of the vortices along the cylinder as a function of distance downstream from the leading edge. (*a*) Various chord-to-thickness ratios in the natural shedding case; (*b*) various forcing frequencies at a chord-to-thickness ratio of $c/t = 8$; (*c*) various cylinder lengths with forcing frequency at $St_{ft} = 0.16$. $Re = 400$ and $v_{pert} = 2.5\%$.

0.14, 0.165, 0.174 and 0.19. The forcing frequency is fixed at $St_{ft} = 0.16$ in figure 8(*c*) showing the convective velocities for $c/t = 7, 9, 11, 13$ and 15.

A general trend is observed in all these cases regardless of chord-to-thickness ratio and forcing frequencies (when forcing is applied). Perhaps this is not surprising given

the low level of forcing. The convective velocity reaches a minimum close to the time
the vortex is fully formed. After separating from the shear layer, it then accelerates
and reaches semi-equilibrium at approximately 70% of the free-stream velocity.

There are a few notable differences. The minimun convective velocity moves from
approximately $4t$ to $2t$ from the leading edge when forcing is applied. This is a result of
the applied forcing causing the reattachment length to shorten significantly. There are
also other exceptions in natural shedding cases. The deviation of the shortest chord-
to-thickness ratio ($c/t = 6$) from the others is probably due to the close proximity of
the trailing edge. The scatter seen for $c/t = 8$ is caused by flow that is not perfectly
periodic, i.e. every period is not exactly identical.

### 3.4.3. *Phasing of the trailing-edge shedding*

The next step is to investigate the trailing-edge shedding and how this relates to
the mean base pressure. First, the flow for $c/t = 10$ is examined in detail. Next, the
cylinder with $c/t = 8$ is investigated because it is typical of the cylinders that have
two local peaks in the mean base suction within the lock-in range. Finally, vorticity
plots for the whole range of cylinders studied show the similarities of the flow at the
trailing edge when the mean base suction peaks.

Figure 9 shows vorticity plots for $c/t = 10$ at $St_{ft} = 0.12, 0.15, 0.165$ and $0.18$ together
with the plot of mean base pressure as a function of the forcing frequency. Only plots
taken at $0°$ and $90°$ in the forcing cycle are shown. The other half of the cycle
mirrors these plots because the flow is locked and therefore periodic. These leading-
edge vortices convect downstream and control the shedding at the trailing edge, as
the trailing-edge vortices are formed from the attached boundary layer between the
passing of leading-edge vortices. As the forcing frequency is increased from $St_{ft} = 0.12$
to $St_{ft} = 0.165$, the gradual increase in mean base suction is associated with a gradual
change (retardation) in the phase of the trailing-edge shedding relative to the forcing.
As the forcing frequency is incremented to $St_{ft} = 0.18$, there is a more drastic decrease
in the mean base suction. The vorticity plot shows that the higher forcing frequency
suppresses the trailing-edge shedding, which is consistent with the associated decrease
in mean base suction.

Figure 10 shows the vorticity plot for $c/t = 8$ for forcing frequencies of $St_{ft} = 0.14$
and $St_{ft} = 0.174$, which correspond to the two local peaks in the mean base suction.
Also shown is the variation of the mean base pressure as a function of forcing
frequency. At the forcing frequency of $St_{ft} = 0.14$, the phase of the trailing-edge
shedding relative to the forcing is similar to the case where the chord-to-thickness
ratio is $c/t = 10$ and the forcing frequency is $St_{ft} = 0.165$; both cases show a peak in
the mean base suction. When the forcing frequency is at $St_{ft} = 0.174$, the shedding
from the trailing edge is approximately $180°$ out of phase relative to the shedding at
the lower forcing frequency ($St_{ft} = 0.14$). As the shedding in this case is only half a
cycle ahead of the previous case and not a complete cycle ahead, these frequencies
correspond to the intermediate step between shedding modes shown in figure 7.

To demonstrate that the observations for cylinders with $c/t = 10$ and $8$ are
representative of the different cylinder lengths studied, figure 11 shows the vorticity
patterns corresponding to every local peak in mean base suction. These are taken
at $0°$ in the forcing cycle. They correspond to the same chord-to-thickness ratios
and Strouhal numbers plotted in figure 5, which shows the stepwise behaviour.
For the cases corresponding to the primary peaks, the shedding at the trailing edge
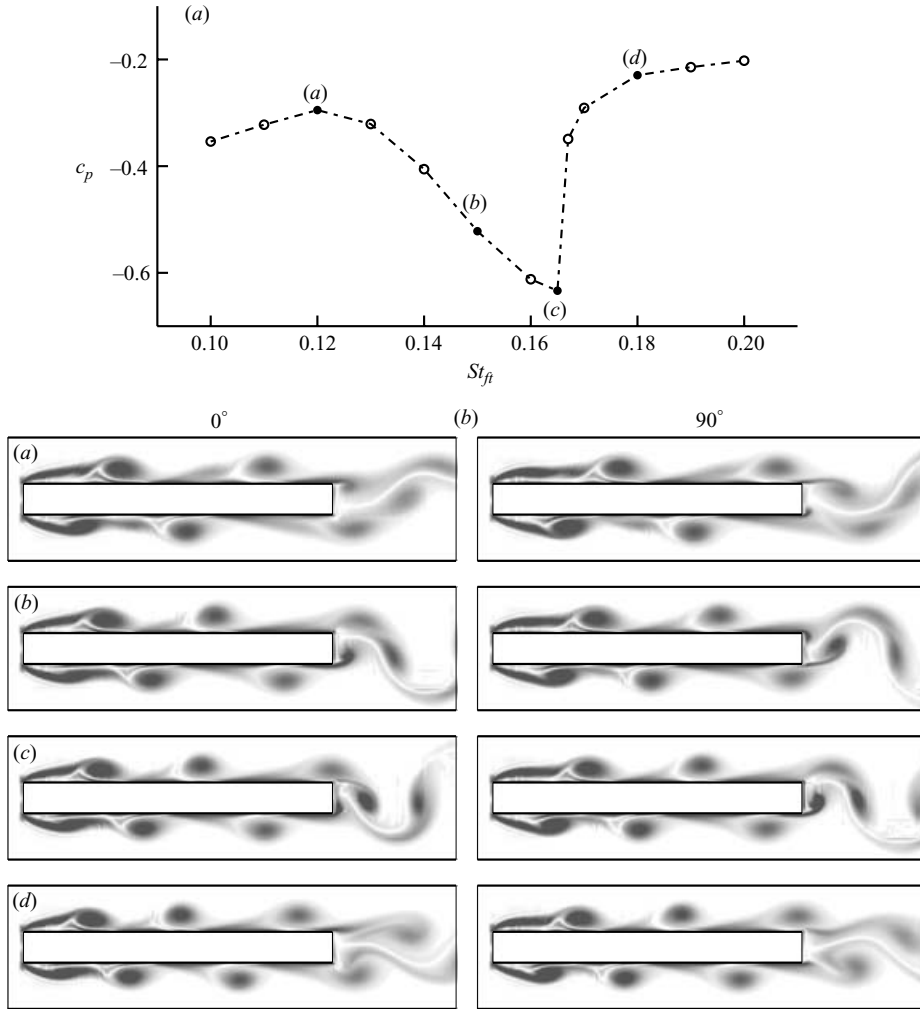shows approximately the same relative phasing. In contrast, the trailing-edge shedding

FIGURE 9. (*a*) The mean base pressure coefficient as a function of forcing frequency. (*b*) Vorticity contours for flow over a cylinder with $c/t = 10$, $Re = 400$ at $0°$ and $90°$ in the forcing cycle at forcing frequencies of (*a*) $St_{ft} = 0.12$, (*b*) 0.15, (*c*) 0.165 and (*d*) 0.18 with an amplitude of $v_{pert} = 2.5\%$.

corresponding to secondary peaks is $180°$ out of phase. The vorticity plots in figure 11 clearly show the different shedding modes that correspond to the Strouhal number steps in figure 5. For the primary cases, the local peaks corresponds to $c/t = 6$, 7, 8 and 9; $c/t = 10$, 11, 12 and 13; and $c/t = 15$ and 16, for shedding modes $n = 2$, 3 and 4, respectively. For the secondary cases, $c/t = 8$ and 9 and $c/t = 12$, 13 and 14 correspond to modes between $n = 2$ and 3, and $n = 3$ and 4, respectively.

### 3.5. *The vortex formation length past the trailing edge*

In §§3.1 and 3.2, we see that some local primary peaks in mean base suction are more significant in both the simulated and experimental data. The previous subsection has shown that the phase of the trailing-edge shedding relative to the forcing is
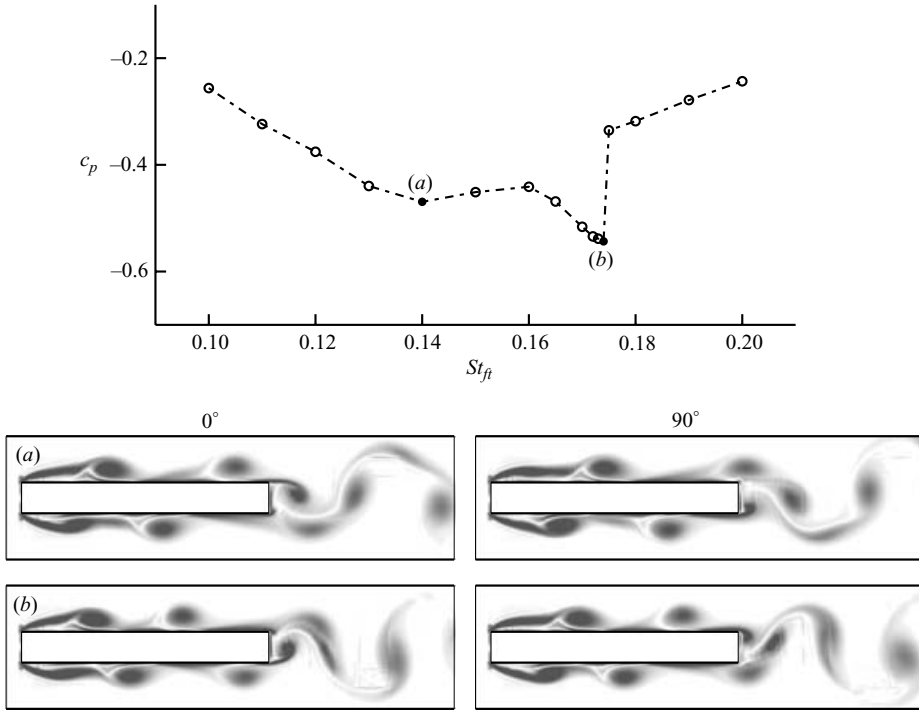
FIGURE 10. (*a*) The mean base pressure coefficient as a function of forcing frequency. (*b*) Vorticity contours for flow over a cylinder with $c/t = 8$, $Re = 400$ taken at $0°$ and $90°$ in the forcing cycle at forcing frequencies of (*a*) $St_{ft} = 0.14$ and (*b*) 0.174 and $v_{pert} = 2.5\%$.

approximately the same in all these cases. The vortex formation length is calculated for a selection of cases to show the direct connection between the mean base suction and the trailing-edge shedding.

The vortex formation length has been calculated for cylinders with chord-to-thickness ratios of $c/t = 8$ and 10. Also included for comparison are results for a cylinder with an elliptical leading edge with a chord-to-thickness ratio of $c/t = 7.5$ and a 5:1 axis-ratio half-ellipse for the nose. The standard deviation of the cross-flow component of velocity is determined along the centreline downstream of the trailing edge of the cylinder. The vortex formation length is taken to be the distance downstream where the fluctuating component of the velocity in the cross-flow direction reaches a maximum. Plots of the vortex formation length and mean base pressure as a function of forcing frequency for the three different cylinders are shown in figure 12.

The elliptical leading-edge cylinder shows approximately a linear relationship between the mean base pressure and the vortex formation length, although over a much narrower range, as the flow only locks on to this range for this level of forcing. In this case, there is no leading-edge shedding and the base shedding can be seen to be very sensitive to forcing frequency as reflected in the vortex formation length and mean base pressure. For most of the frequency range, there is also a direct relationship between the vortex formation length and the mean base pressure for the rectangular cylinder; however, it is not maintained at high forcing frequencies where the trailing-edge shedding is suppressed.
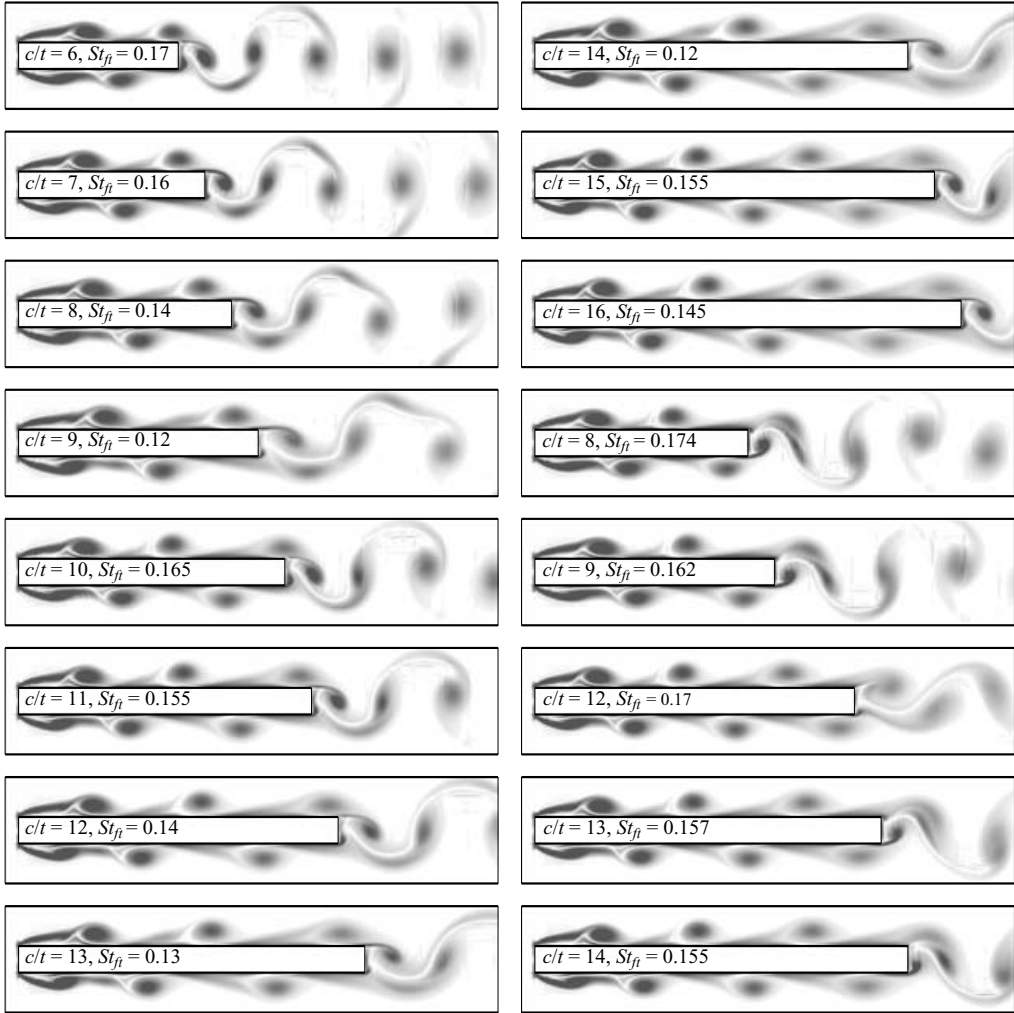
FIGURE 11. Vorticity plots for cylinders with forcing frequencies chosen so as to result in local maxima in the mean base suction as a function of forcing frequency. The plots are taken at $0°$ in the forcing cycle. All plots in the left column and top three plots in the right column correspond to *primary* peaks and bottom five plots on the right correspond to *secondary* peaks.

## 4. Discussion

### 4.1. *Validity of parameter choices*

Initially, modelling issues will be discussed in this section, including the effect of forcing amplitude and the influence of Reynolds number. The presence of the natural (ILEV) instability at these low Reynolds numbers is also discussed.

#### 4.1.1. *Effect of Reynolds number*

To study the effects of Reynolds number, the flow for $c/t = 10$ and $v_{pert} = 2.5\%$ was simulated at $Re = 300$, 400 and 500. Note that for the unforced case at $Re = 300$ the rollup of the leading-edge shear layer is very much weaker than occurs at the higher Reynolds numbers. Despite this, varying the Reynolds number had only a small effect on mean base pressure and did not change the overall observed trends
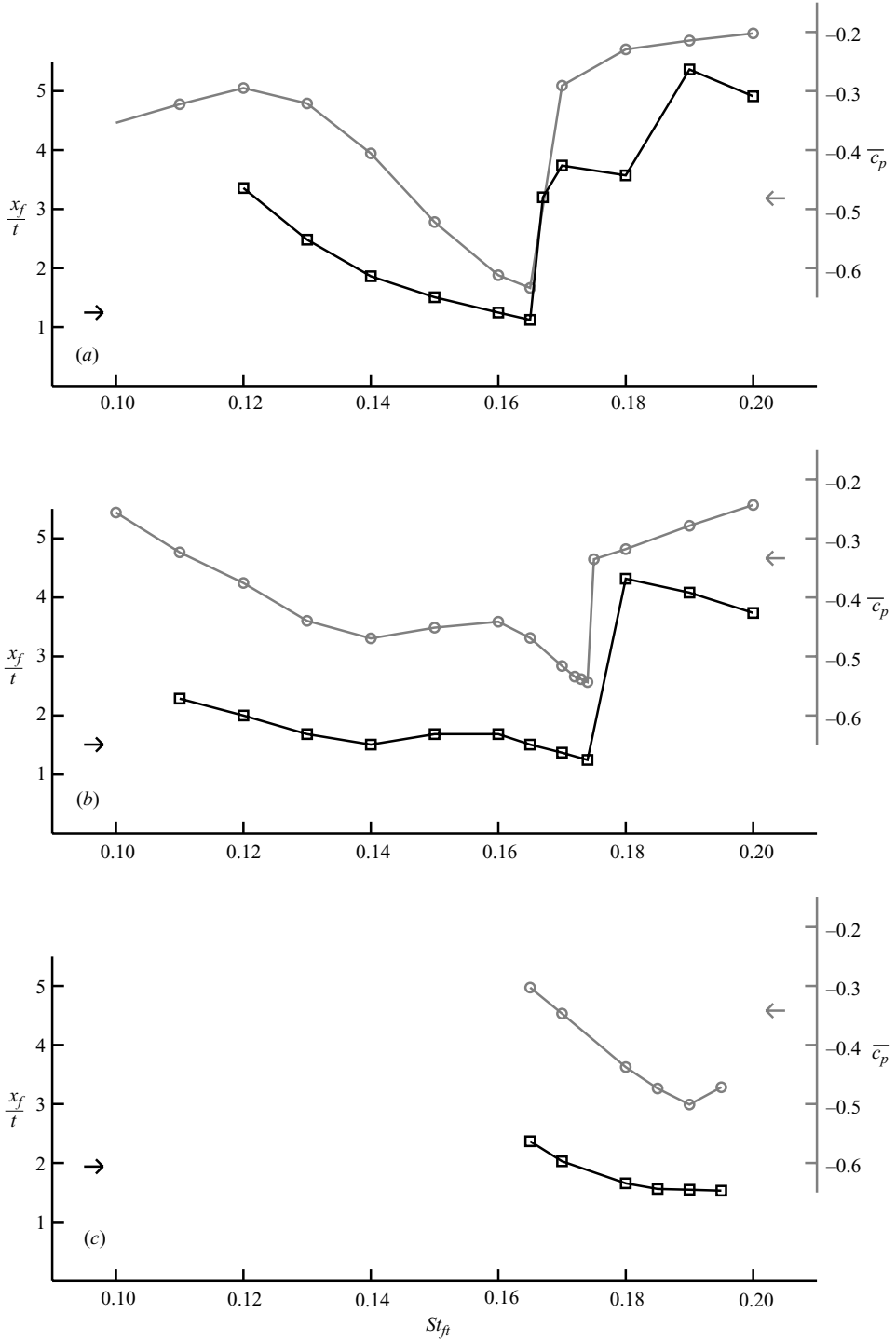
FIGURE 12. Vortex formation lengths (grey lines) and mean base pressure coefficient (black lines) as a function of forcing frequency for (*a*) $c/t = 8$, (*b*) $c/t = 10$, and (*c*) an elliptical leading-edge cylinder with $c/t = 7.5$. $Re = 400$ and $v_{pert} = 2.5\%$ in all cases. Black and grey arrows show the vortex formation length and the mean base pressure respectively when no forcing is applied.

for the range of forcing frequencies simulated ($0.08 \leqslant St_{ft} \leqslant 0.28$). The flow locks to the forcing over a large frequency range in these cases (e.g. for $c/t = 10$, $Re = 400$ and $v_{pert} = 2.5\%$, the lock-in range was $0.12 \leqslant St_{ft} \leqslant 0.23$). Increasing the Reynolds number did not significantly alter the forcing frequency at which the peak in mean base suction occurred but marginally increased the magnitude of the peak.

### 4.1.2. *Effect of forcing level*

The forcing level applied at the computational boundaries was generally chosen as $v_{pert} = 2.5\%$. Simulations were performed without the mean free-stream component to determine the effective forcing level near the cylinder. The perturbation amplitude was monitored at three locations near the corners of the cylinder, i.e. (i) $0.5t$ horizontally away, (ii) $0.5t$ vertically away, and (iii) $0.5t$ both vertically and horizontally away from the sharp edge. The perturbation level near the cylinder increased linearly by approximately 2% relative to the free-stream velocity when the chord-to-thickness ratio is increased from $c/t = 6$ to 16. This is due to the increase in blockage in the cross-flow direction.

Although the difference in effective forcing level near the cylinder appears large as the chord-to-thickness is varied, further simulations have shown that this system is not sensitive to forcing levels once the flow is locked. These simulations were performed with $v_{pert} = 1.25\%$ for a range of chord-to-thickness ratios and forcing frequencies. Reducing $v_{pert}$ by 50% results in a larger variation in forcing level near the cylinder compared with varying the chord-to-thickness ratio, $c/t$, for a fixed $v_{pert}$. The simulations with a lower forcing amplitude shows the same trends in mean base suction with only a small quantitative difference, in particular, the magnitude of the primary peaks decreases marginally. The only significant variation would be the amplitude of the secondary peaks in mean base pressure, which appear larger when the forcing amplitude is reduced.

### 4.2. *The natural instability*

The natural feedback loop can lock the leading- and trailing-edge shedding in the absence of external forcing at the Reynolds numbers used in these simulations (see Hourigan *et al.* 2001). However, as the feedback loop is weak, a low-level oscillatory forcing is able to lock the flow over a wider range of frequencies (details are presented in §3.1), overpowering the natural feedback loop.

The effect of the ILEV mechanism for the natural shedding case is evident when comparing the mean base pressures and drag forces between the forced and unforced cases (figures 3 and 4). In the forced cases, the forcing frequency at which the mean base pressure reaches a minimum (equivalent to maximum base suction) does not coincide with the natural shedding frequency, although the discrepancy is generally not large. The frequency selection will be shown in §4.4 to be governed by the convective velocity of the vortices along the cylinder. Through figure 8 it has already been shown that there are some differences in convective velocities between the forced and unforced cases. The discrepancy in frequency, although small, strongly influences the trailing-edge shedding (see §4.5), and results in the differences in mean base pressure between the local peaks in the forced and the unforced cases. The applied forcing alters the characteristics of the mean drag relative to the unforced case in a manner similar to the mean base pressure.

### 4.3. *Comparison with experimental results*

The forcing levels in the experimental study (Mills *et al.* 1995, 2002; Mills 1998) were measured near the cylinder in the absence of the mean flow. The amplitude

was measured at $0.1t$ vertically away from the edge of the cylinder for $c/t = 10$; a level of 5% relative to the free stream was determined and kept constant for the other chord-to-thickness ratios examined. This level of forcing can be achieved in the simulations when $v_{pert}$ is between 1.25% and 2.5% of the free-stream velocity. As discussed earlier, the simulations are not sensitive to forcing amplitude at these levels of forcing.

The behaviour of the primary peaks in mean base suction seen in figure 3 for the simulated flows is also seen in the the experimental data of Mills (1998) and Mills *et al.* (2002). Although there is substantial agreement between the predictions and the experimental results, there are also several differences between the two sets of data. The most noticeable is the different scale used for both axes. For the frequency range, the one used for the simulations is chosen to fully capture the lock-in range. For the experimental data, the lower limit in frequency is determined by an experimental limitation and there is little variation from the unforced case past $St_{ft} = 0.20$.

Besides the quantitative differences there are a couple of distinct trends in the numerical and experimental data. The first one concerns the variation in the magnitude of the peaks in mean base pressure. In the simulations, local primary peaks in mean base suction appear to be larger when they occur at higher forcing frequencies. The experimental data show larger values of mean base pressure when the peaks occur at an intermediate frequency. This is governed by the response of trailing-edge shedding to these forcing frequencies and will be discussed further in §4.5.

The height of the steps between the the shedding modes shown in figure 5 is another significant difference between the experimental and numerical results. The steps in the simulation are approximately $St_{fc} = 0.55n$ while for the experiments they are approximately $St_{fc} = 0.6n$. This difference is also present in the natural shedding case when comparing simulated (Hourigan *et al.* 2001) and experimental (Nakamura *et al.* 1991) data. The discrepancy is addressed together with the frequency selection mechanism in §4.4.

Just to recap, there are distinct differences between the experiments and numerical model that are likely to cause these differences. The simulations are performed in two dimensions at $Re = 400$ while for the experiments $Re \approx 9000$. Although the applied forcing suppresses three-dimensionality in the flow field, it is present at higher Reynolds numbers together with the two-dimensional spanwise vortex rollers (Hourigan *et al.* 1993). In addition, but less important, there are differences in the way the forcing is generated and the induced perturbation field near the cylinder meaning that the forcing fields only approximate each other.

### 4.4. *Phasing of the leading- and trailing-edge shedding relative to forcing*

Some of the vorticity plots shown earlier are re-examined in this section to investigate the phase relationship between the leading- and trailing-edge shedding, and the forcing. All vorticity plots shown in this study, with a detailed illustration in figure 7, show that the phase of shedding from the leading edge relative to the forcing is constant once the flow is locked. The top shear layer is in the initial stages of forming a vortex at 180°. This vortex then gains more circulation from the shear layer at 270°. It starts to detach at 0° and by 90°, it is almost completely shed from the shear layer. The shedding from the bottom is 180° out of phase with the top. In all cases, the vortex on the top of the cylinder forms between 90° and 270° in the forcing cycle; this is when the transverse perturbation is accelerating in the downward direction. The forcing is therefore causing a more compact vortex to form closer to the leading edge relative to the natural shedding case. During the other half of the cycle, the

acceleration upward helps shed the vortex. This phase relationship is likely to be the most beneficial to the shedding process resulting in the constant phase relationship between the shedding and the forcing for all the cases.

The phase of the trailing-edge shedding relative to the forcing is governed primarily by the forcing frequency and chord-to-thickness ratio. In §3.4.2, it was shown that the convective speed of vortices along the cylinder is not sensitive to various parameters. Noting that the trailing-edge vortices are shed between the passing of leading-edge vortices, increasing the forcing frequency gives less time between periods for the leading-edge vortices to travel downstream and therefore retards the phase of the leading-edge vortices on arrival at the trailing edge. Increasing the chord-to-thickness ratio also retards the phase of the trailing-edge shedding because of the larger distance for the leading-edge vortices to travel before reaching the edge of the cylinder. This is illustrated in figure 11 where within each of the various shedding modes, the forcing frequency decreases with chord-to-thickness ratio to keep the phase of the shedding constant at the trailing edge. To maintain the same phase of trailing-edge shedding, the effect of decreasing the forcing frequency and advancing the phase must be matched with the retarding of the phase caused by increasing the chord-to-thickness ratio.

All the primary local peaks in mean base suction for the various chord-to-thickness ratios share a similar phase of the trailing-edge shedding relative to the forcing. The secondary local peaks also share a common phase, approximately 180° shifted relative to the primary peaks. The trailing-edge shedding for a case associated with the primary peak is shown in figure 9(c) ($c/t = 10$ and $St_{ft} = 0.165$) and figure 11 (primary peaks). There are similarities between the phases of the leading- and trailing-edge shedding in this case. At 0° in the forcing cycle, both the leading- and trailing-edge vortices are forming on the top side of the cylinder while on the bottom of the cylinder, the vortices have been shed from both the leading and trailing edges. At 90° into the forcing cycle, both shedding processes are still at a similar phase in that the vortices on the bottom side are just forming while the top ones are about to be shed. Overall, vortices on the top half of the cylinder form approximately between 90° and 270° in the cycle when the perturbation velocity is accelerating in the downward direction and the opposite occurs during the other half of the cycle. This raises another possible reason for the strong base suction besides the resonance resulting from the similarity in shedding phase between the leading and trailing edge. The forcing is assisting the trailing-edge vortices to form closer to the centreline of the cylinder. A stronger base suction is then a result of the vortices forming closer to the base. It is not surprising then that increasing the forcing level increases the magnitude of these local peaks.

The phase of the shedding relative to the forcing for the secondary local peak is illustrated in figure 10 ($c/t = 8$ and $St_{ft} = 0.174$) and figure 11 (secondary peaks). Although the secondary peaks in mean base suction are generally weaker at these intermediate steps, there is still some resonance that causes the stronger mean base suction. Simulations at a lower forcing level of $v_{pert} = 1.25\%$ have consistently shown that contrary to the behaviour of the main peaks in mean base suction, the magnitude of these secondary peaks decreases with increasing forcing amplitude. In this case, the opposite of the earlier case is occurring. The forcing field is causing the trailing-edge vortices to form further away from the centreline and cylinder base, and therefore increasing the forcing level results in a reduction in base suction.

### 4.5. *Frequency selection and the stepping in the natural and forced shedding cases*

An earlier study by Hourigan *et al.* (1993) hypothesized that the control (stepping) of the mean base suction was due to the leading-edge vortices passing the trailing

edge and interfering with the base shedding. This study, together with Hourigan *et al.* (2001) for the natural shedding case, supports this hypothesis by revealing the details involved in this interaction. The visualizations presented in this paper clearly show that trailing-edge vortices form between the passing of leading-edge vortices. In both the natural shedding case and for the flow corresponding to the primary peaks for the forced case, the leading- and trailing-edge shedding is synchronized. As the average convective velocity has been shown to be approximately constant, the frequency must decrease with increasing chord-to-thickness ratio to allow more time for the vortex to traverse the cylinder and maintain the synchronization. This continues until the flow is no longer receptive to the low frequency. While this is happening, another higher frequency within the lock-in range is excited. Here the synchronization between the leading and trailing edge is maintained but now an additional pair of vortices exists along the cylinder. The frequency is higher because less time is needed in each period as the leading-edge vortices take an extra period to reach the trailing edge. This is associated with the next higher shedding mode and a jump to the next step in the frequency selection diagram. As the chord-to-thickness ratio is increased further, this process repeats itself for the remaining steps.

In both the natural shedding and forced cases, the steps in frequency of the vortex shedding and peak time-mean base pressures, respectively, correspond to approximately $St_c = 0.55n$. The Strouhal number based on chord is the frequency multiplied by the chord and divided by the free-stream velocity. Consider the first mode ($n = 1$). The frequency is the inverse of the time taken by a leading-edge vortex to travel the chord. Therefore, the Strouhal number based on chord, $St_c$, is the streamwise component of the convective velocity of the leading-edge vortex averaged over the chord and scaled with the free-stream velocity. For the higher modes, the factor $n$ is the number of periods required for a leading-edge vortex to pass the trailing edge. From figure 8, both natural and forced shedding cases show the convective velocity initially reaching a minimum before rising to saturate at about 70% of the free-stream velocity. The levels of the steps indicate that the average convective velocity is about 55% of the free-stream velocity. Both the experiments for the natural shedding case (Nakamura *et al.* 1991) and the forced case (Mills 1998; Mills *et al.* 2002) show a step height of about $St_c = 0.6n$. Differences in Reynolds number and thus three-dimensionality in the experiments may account for this slightly higher average convective velocity.

### 4.6. *Trailing-edge shedding and the vortex formation length*

In §3.1, both the computed and previous experimental results show that the magnitude of the peak base suction varies with chord-to-thickness ratio. The trailing-edge shedding has the same phase relative to the forcing for all cases associated with the primary peaks. This is hypothesized to be most conducive to the shedding process. This frequency is controlled by the time taken for the leading-edge vortices to traverse the cylinder. It is therefore hypothesized that the response of the base shedding to the forcing at the frequency corresponding to peak mean base suction governs the magnitude of the peak mean base suction.

This hypothesis is supported by the results in §3.5 and figure 12. The vortex formation length is a quantifiable measure of the trailing-edge shedding. The vortex formation length is linearly related to the mean base suction when there is no leading-edge shedding in the case with the elliptical leading edge. The similar relationship between the vortex formation length and the mean base suction for the cases with the rectangular cylinder geometry suggests that the base shedding is also responsible for

the observed behaviour in mean base suction when there is leading-edge shedding. As the base shedding is sensitive to frequency for the elliptical leading-edge cylinders, it is also reasonable to assume that the base shedding is sensitive to frequency for rectangular cylinders. While the forcing frequency at which the mean base suction peaks is controlled by a separate mechanism, the resulting magnitude of the peak is governed by how receptive the base shedding is to that particular frequency.

The sensitivity of the base shedding can also explain why the peak mean base suction in the forced case is greater at some chord-to-thickness ratios than the natural shedding case but not others (§ 3.1). In the unforced case, the frequency selection is governed by the ILEV/TEVS instability (Hourigan *et al.* 2001). In the forced shedding case, there are slight differences in the convective velocity and therefore the frequency at which the base suction peaks compared with the unforced case. The response of the trailing-edge shedding to these two frequencies probably accounts for this.

This hypothesis can also be invoked when comparing the magnitudes of the peaks in the simulation and the experiments. In the simulation, the peaks are generally greater when they occur at lower forcing frequencies, while in the experiments they are generally greater at an intermediary frequency. This is probably due to the base shedding being receptive to different frequencies and to the large disparity in Reynolds numbers.

### 4.7. *Suppression of base shedding*

From the mean base pressure plots in figure 3 and mean drag plots in figure 4, there are cases where the mean base suction and drag are below that of the unforced case. Effectively, the base shedding is not receptive to the forcing frequency for this range although the flow is locked. Both the forcing and leading-edge vortices are interfering with the base-shedding process; in some cases the base shedding is significantly reduced or even suppressed. An example of this can be seen in figure 9(*d*) ($c/t = 10$, $St_{ft} = 0.18$). This phenomenon has been observed in experiments using short bluff bodies. Experiments by Bearman & Obasaju (1982), and Ongoren & Rockwell (1988) observed that flow around short bluff bodies oscillated at higher frequencies could reduce the base suction to less than that without forcing.

### 4.8. *Relating the fluctuating lift forces to the flow field*

The Strouhal numbers based on forcing frequency ($St_{fc}$) which result in local peaks in mean drag and local maxima/minima in fluctuating lift force are plotted in figure 5 against chord-to-thickness ratio. The mean drag force mirrors the mean base pressure as expected and shows both the primary and secondary intermediate steps. The Strouhal numbers for the fluctuating lift force also show this stepping behaviour but with local maxima corresponding to the primary steps and local minima to the intermediate secondary steps. The lift force is a function of the pressure on the top and bottom surfaces. The leading-edge vortices represent a low-pressure region on the surface near the vortex. Therefore the fluctuations in the lift force come from the mismatch in vortices on both sides of the cylinder. The leading edge sheds vortices alternately, which contributes to some of the fluctuating lift force. As this occurs similarly for all cylinders and frequencies, it cannot account for the variations in fluctuating lift forces as the forcing frequency is varied. The suction effects of the pairs of vortices along the cylinder approximately cancel each other. Once these vortices pass the trailing edge, their effect on the cylinder is significantly diminished. Therefore, the mismatch leading to fluctuating lift occurs at the trailing edge as the pairs of vortices from the top and bottom pass the trailing edge 180° out of
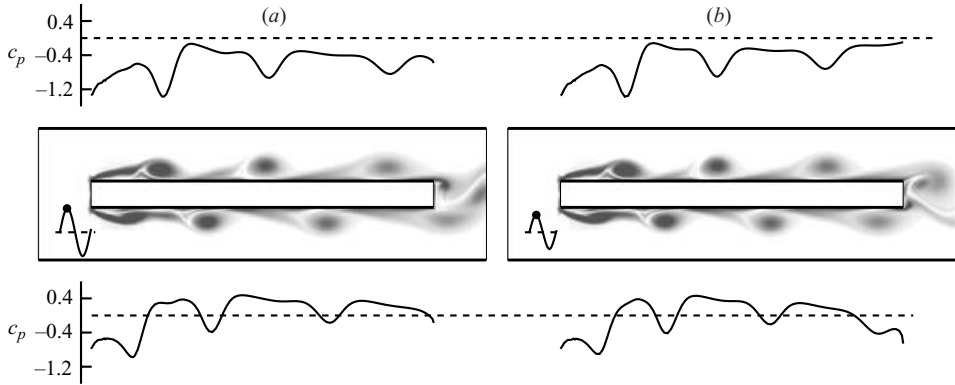
FIGURE 13. Vorticity contours (centre) and surface pressure coefficient on the top and bottom surface (above and below) for $c/t = 13$, $Re = 400$, taken at $0°$ in the forcing cycle with $v_{pert} = 2.5\%$, and (*a*) $St_{ft} = 0.14$ and (*b*) to $St_{ft} = 0.16$. The inset at the bottom left of each vorticity plot is the time trace of the lift coefficient with the dot corresponding to the time of plots. Note the lift force is maximum upwards at $0°$ in the forcing cycle.

phase. For a given chord-to-thickness ratio, the forcing frequency controls the phase relative to the forcing when the vortices pass the trailing edge while the phase of the leading-edge shedding relative to the forcing is fixed. The magnitude of the fluctuating lift force is controlled by the relative phase between the leading-edge shedding and vortices passing the trailing edge since this can lead to reinforcement or cancellation. Maximum superposition occurs in cases associated with the primary steps. For the intermediary secondary steps where the trailing-edge shedding, and therefore the passing of the leading-edge vortices at the trailing edge, is $180°$ out of phase from the earlier case, minimum superposition occurs. Therefore the fluctuating lift, like the mean base pressure and integrated drag force, is also dependent on the phasing of the leading-edge vortices as they pass the trailing edge.

The flow for $c/t = 13$ is used to illustrate the relationship between the timing of vortices passing the trailing edge and the fluctuating lift force. Figure 13 shows vorticity plots taken when the forcing is at $St_{ft} = 0.14$ and 0.16, which correspond to local maxima and minima for the standard deviation of lift coefficient. These plots are taken at $0°$ in the forcing cycle. The time trace of the lift coefficient in both plots is sinusoidal and shows that the lift coefficient reaches a maximum (maximum lift force in the upward direction) at $0°$ in the forcing cycle. This corresponds to the maximum acceleration in the upward direction for the perturbation field. Note that the offset between the top and bottom surfaces of the cylinder is due to the perturbation field. Simulations without any mean flow have shown the pressure fluctuation on the surface of the cylinder to be approximately equivalent to this offset.

The leading-edge shedding occurs at approximately the same shedding phase for both forcing frequencies shown. At the trailing edge, the plot shows that the flows are approximately $180°$ out of phase. As a result, there are three pairs of vortices for the $St_{ft} = 0.16$ case but only two pairs plus an unpaired vortex on the top side when $St_{ft} = 0.14$ (neglecting the partially formed vortex on the bottom side of the leading edge in both cases). For the case when $St_{ft} = 0.14$, the extra vortex on the top side increases the lift coefficient in the upward direction because each vortex is associated with a low pressure region. When $St_{ft} = 0.16$, the vortices are paired and this results in a lower lift coefficient. As these are extreme cases with respect to the fluctuating lift force, other forcing frequencies result in intermediate lift coefficient values.
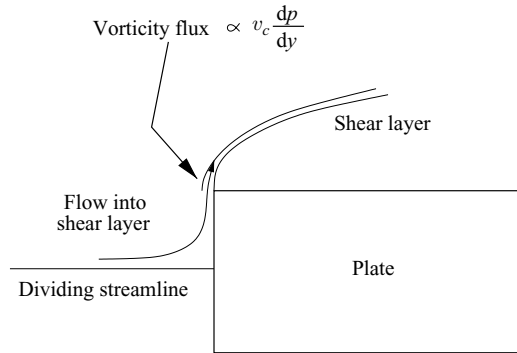
FIGURE 14. Representation of the formation of the separating shear layer through convection of leading-edge vorticity.

### 4.9. *The relative roles of ILEVs and TEVs in the feedback process*

The important role of the trailing-edge shedding in governing the flow response to applied forcing has been shown. This subsection attempts to highlight the importance of the trailing-edge shedding when no forcing is applied.

The original explanation for the Strouhal number stepping with chord-to-thickness ratio for the unforced flow was through the impinging shear layer instability (ISLI) or, perhaps more accurately, the impinging leading-edge vortex (ILEV) instability mechanism (Nakamura *et al.* 1991; Mills *et al.* 1995), whereby leading-edge vortices passing the trailing edge of the cylinder induce a pressure fluctuation which perturbs the leading-edge shear layer hence controlling the timing of release of the next leading-edge vortex. Thus a feedback loop is established. That mechanism has been hypothesized to be responsible for a range of resonant phenomena such as cavity resonances (e.g. Rockwell & Naudascher 1979). More recently, it has been conjectured that trailing-edge vortices (TEV) play a much stronger role in the feedback loop than previously believed (Hourigan *et al.* 2001). A couple of features of the observations have led to this view. First, the early experimental visualizations of the locked flow did not show any strong base shedding (Mills *et al.* 1995). This now appears to have been a seeding problem with the visualizations, i.e. a failure to feed smoke, dye or hydrogen bubbles into the region near the trailing edge, and hence the strong trailing-edge shedding was overlooked. Secondly, the lengths of the Strouhal number steps in this case are quite short, more consistent with the narrow frequency band over which the trailing-edge shedding is receptive, than the relatively wide band for leading-edge shedding (Soria *et al.* 1993; Wu & Soria 1992). However, the evidence supporting a strong role for TEVs in the feedback loop was still circumstantial.

One of the advantages of numerical simulations is the ability to investigate separate effects through various means that are difficult or impossible to do experimentally. To determine the relative roles of TEVs and ILEVs in the feedback process, the induced pressure fluctuation at the leading-edge shear layer for both processes needs to be quantified. An attempt to isolate the effects is described below.

A numerical simulation was performed for a representative unforced case for $c/t = 10$. For this chord-to-thickness ratio the locking is strong. The flow was evolved until it had reached its periodic, asymptotic state. The flux of vorticity into the leading-edge shear layer depends on the product of the pressure gradient $dp/dy$ and convection velocity $v_c$ at the leading-edge corner (Morton 1984) as shown in figure 14. Here, $y$ is measured along the front face. The convection velocity is representative
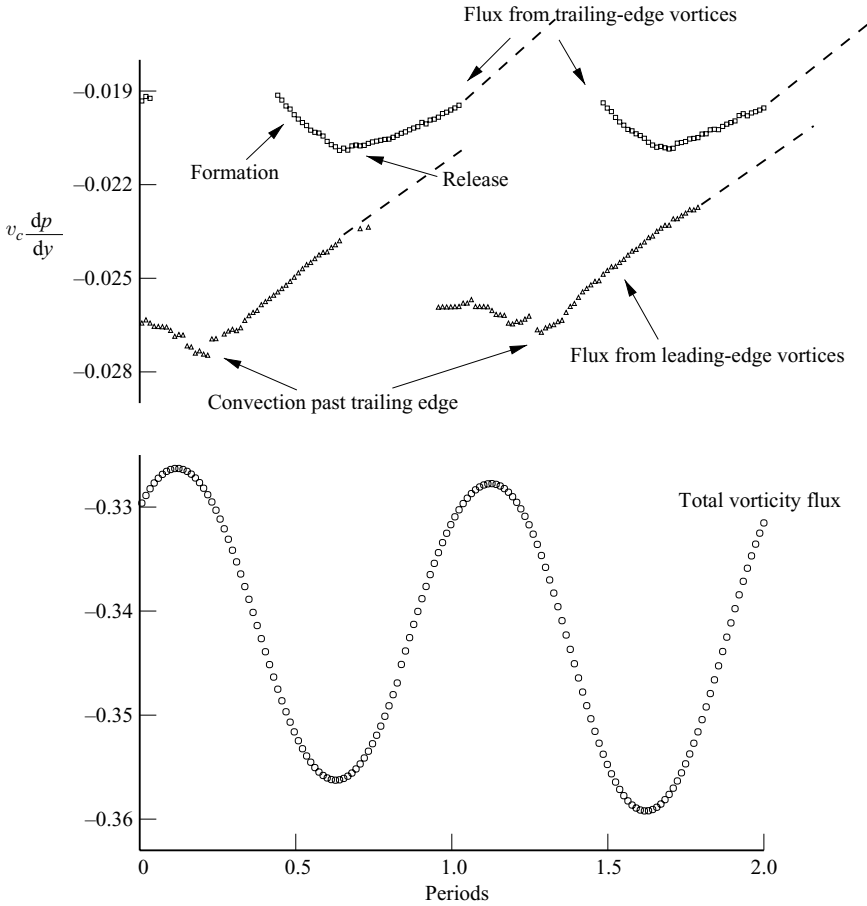
FIGURE 15. Variation of vorticity flux into the separating shear layers from convecting leading-edge vortices, trailing-edge vortices and measured total flux. $Re = 400$, $c/t = 10$.

of the mean velocity through the boundary layer. In this case it was measured at a horizontal distance of $0.2t$ from the top corner. While the exact positioning affects the magnitude of the recorded flux it has little effect on the oscillatory component, which is important as shown by the following argument. Both $dp/dy$ and $v_c$ were recorded directly from the numerical simulations. The flux varies about a non-zero mean value with a small-amplitude, approximately sinusoidal oscillation as shown in figure 15. Next the simulation is used to isolate the individual effects on the vorticity flux into the leading-edge shear layer of (i) the passage of leading-edge vortices past the trailing edge, and (ii) the formation and release of the trailing-edge vortices into the wake. This is done by recording the position of the maximum vorticity for both vortex types as a function of time for approximately two cycles. Simultaneously, the total circulations of both types of vortex were also recorded. Although there is some arbitrariness in the spatial extent of the vortices when computing the circulations, this does not affect the main conclusions given below.

A complex mapping using the Schwarz–Christoffel transformation (e.g. Churchill, Brown & Verhey 1974) can be used to calculate the potential flow past a long cylinder by transforming the cylinder to the interior of a circle. By mapping the geometry to a circle, the positions and strengths of image vortices within the circle are known

so that the boundary conditions at the surface of the body are satisfied. Using the transformation, and the positions and circulations recorded from the simulation, and treating the vortices as potential-flow point vortices, it is thus possible to calculate the potential flow velocity and pressure distribution throughout the domain. In particular, this allows the vorticity flux into the leading-edge shear layer to be estimated owing to the presence of uniform background flow, and leading-edge and trailing-edge vortices. This has been done for both forming and shedding trailing-edge vortices, and convecting leading-edge vortices.

The results are shown in figure 15. The time variation of the vorticity flux from the trailing-edge vortices is correlated well with the measured flux variation, clearly showing the same phasing. In contrast, the flux contribution from the passage of the leading-edge vortices past the trailing edge is not well correlated with the measured flux. This phasing seems to indicate that the ILEV contribution to the feedback loop is less important than the TEV component. These curves have been truncated when the leading- and trailing-edge vortices begin to merge in the wake. The dashed lines show the approximate effect as the merged vortices are convected further downstream. For the leading-edge vortices, the flux contribution is only recorded when they are within a few cylinder thicknesses from the trailing edge. The dip in the curves for the leading-edge vortices occurs when they pass the trailing edge, while the peak for trailing-edge vortices corresponds to the time when a vortex has reached maximum strength and is beginning to be shed downstream. Note that the size of the perturbation to the vorticity flux is relatively small for both the leading- and trailing-edge vortices; the total flux variation is due to the time variation of all the vorticity in the field and is especially influenced by vorticity near the leading edge.

## 5. Conclusions

The forced flow around long rectangular cylinders has been simulated for a wide range of parameters. The Strouhal numbers based on chord for the primary peaks in base suction are in good agreement with experimental results for the forced case. In addition, they correspond well with natural Strouhal numbers for the unforced simulations.

A detailed investigation has been performed to identify the physical mechanism leading to this correspondence. The simulations show that the phase of the leading-edge shedding relative to the forcing is insensitive to chord-to-thickness ratio and forcing frequency. In addition, downstream of the leading-edge separation bubble, the convective velocity is also relatively insensitive to variation of the same parameters. The phase of the trailing-edge shedding relative to the forcing is then shown to control the mean base pressure and hence drag. Trailing-edge vortices can only form between the passing of leading-edge vortices and because of this, either increasing the forcing frequency or the chord-to-thickness ratio retards the phase of the base shedding. The peaks in mean base suction all occur when the base shedding is at a similar phase for the various chord-to-thickness ratios and this leads to the stepping in the frequency selection and the various modes ($n$). With the frequency selection accounted for, the magnitude of the base suction peaks is attributed to the sensitivity of the base shedding to those frequencies. Hourigan *et al.* (2001) has also suggested the importance of base shedding in the natural shedding case. By isolating the effects of ILEVs and TEVs, this paper presents evidence that the trailing-edge shedding plays the significant role in the feedback mechanism. In particular, the influence on the leading-edge shear layer of both the formation and shedding of trailing-edge

vortices, and convecting leading-edge vortices, is quantified. The narrowness of the frequency band over which trailing-edge shedding is receptive to external forcing has a strong influence in controlling the length of the Strouhal number steps. In contrast, for situations where there is no trailing-edge shedding, such as for cavity resonances (Rockwell & Naudascher 1979), and bodies with splitter plates (Nakamura 1996), the steps are much longer, since the leading-edge shear layer is receptive over a much broader frequency band.

The feedback process for flow locking and Strouhal number stepping can be described as follows. The narrow-band absolute instability of the trailing-edge shedding controls the selection of the Strouhal numbers of the steps. The Strouhal number based on thickness ($St_t$) is centred on the natural Strouhal number for the base shedding. The perturbation to the leading-edge shear layer, leading to leading-edge vortex shedding, is correlated with the formation and release of the trailing-edge vortices. This perturbation locks the leading-edge shedding to the trailing-edge shedding. These leading-edge vortices also play a significant role. Trailing-edge vortices can only form between the passing of leading-edge vortices, hence the formation of strong trailing-edge vortices, and thus strong base suction, are only possible for certain chord-to-thickness ratios. This is because the convection velocity of leading-edge vortices is approximately constant once they are released from the leading-edge shear layer.

The same frequency selection process is also controlling the fluctuating lift force. In this case the unbalanced leading-edge vortices passing the trailing edge of the cylinder appear to cause the fluctuations.

The mechanisms responsible for the variation of mean drag and the fluctuating lift have been scrutinized in this study. In terms of potential applications, other studies have shown that it is possible to substantially increase the heat transfer rate from heated plates by reducing the reattachment length (Cooper, Sheridan & Flood 1986). While the external forcing reduces the reattachment length, with careful selection of chord-to-thickness ratio and/or applied frequency, the drag penalty can be avoided while also reducing the fluctuating lift forces.

## REFERENCES

BEARMAN, P. W. 1984 Vortex Shedding from Oscillating Bluff Bodies. *Annu. Rev. Fluid. Mech.* **16**, 195–222.

BEARMAN, P. W. & DAVIES, M. E. 1977 The flow about oscillating bluff structures. *Proc. Fourth Intl Conf. on Wind Effects on Buildings and Structures, Heathrow, UK* (ed. K. J. Eaton), pp. 285–295. Cambridge University Press.

BEARMAN, P. W. & OBASAJU, E. D. 1982 An experimental study of pressure fluctuations on fixed and oscillating square-section cylinders. *J. Fluid Mech.* **119**, 297–321.

BLACKBURN, H. & HENDERSON, R. 1996 Lock-in in simulated vortex-induced vibration. *Expl Thermal Fluid Sci.* **12**, 184–189.

CHERRY, N. J., HILLER, R. & LATOUR, M. E. M. P. 1984 Unsteady measurements in a seperated and reattaching flow. *J. Fluid Mech.* **144**, 13–46.

CHURCHILL, R. V. BROWN, J. W. & VERHEY, R. F. 1974 *Complex Variables and Applications*, 3rd Edn. McGraw-Hill.

COOPER, P. I., SHERIDAN, J. & FLOOD, G. J. 1986 The effect of sound on forced convection over a flat plate. *Intl J. Heat Fluid Flow* **7**, 61–68.

GRIFFIN, O. M. 1981 Universal similarity in the wakes of stationary and vibrating bluff structures. *Trans. ASME: J. Fluids Engng* **103**, 52–58.

HOURIGAN, K., MILLS, R., THOMPSON, M. C., SHERIDAN, J., DILIN, P. & WELSH, M. C. 1993 Base pressure coefficients for flows around rectangular cylinders. *J. Wind Engng Indust. Aerodyn.* **49**, 311–318.

HOURIGAN, K., THOMPSON, M. C. & TAN, B. T. 2001 Self–sustained oscillations in flows around long blunt plates. *J. Fluids Struct.* **15**, 387–398.

JOHNSON, S. A., THOMPSON, M. C. & HOURIGAN, K. 2001 Flow past elliptical cylinders at low Reynolds numbers. *14th Australasian Fluid Mechanics Conf., Adelaide University, Australia, 10–14 December 2001* (ed. B. Dally), vol. 1, pp. 343–346.

KARNIADAKIS, G. E. & TRIANTAFYLLOU, G. S. 1989 Frequency selection and asymptotic states in laminar wakes. *J. Fluid Mech.* **199**, 441–469.

LOFTY, A. & ROCKWELL, D. 1993 The near-wake of an oscillating trailing edge: mechanisms of periodic and aperiodic response. *J. Fluid Mech.* **251**, 173–201.

MILLS, R. H. 1998 Vortex interaction in flows over bluff bodies. PhD Thesis, Dept. of Mechanical Engineering, Monash University, Melbourne, Australia.

MILLS, R., SHERIDAN, J. & HOURIGAN, K. 2002 Response of base suction and vortex shedding from rectangular prisms to transverse forcing. *J. Fluid Mech.* **461**, 25–49.

MILLS, R., SHERIDAN, J., HOURIGAN, K. & WELSH, M. C. 1995 The mechanism controlling vortex shedding from rectangular bluff bodies. *Proc. 12th Australasian Fluid Mechanics Conf., 10–15 December, Sydney Unviersity, Australia* (ed. R. W. Bilger), 227–230.

MORTON, B. R. 1984 The generation and decay of vorticity. *Geophys. Astrophys. Fluid Dyn.* **28**, 277–308.

NAKAMURA, Y. 1996 Vortex shedding from bluff bodies with splitter plates. *J. Fluids Struct.* **10**, 147–158.

NAKAMURA, Y., OHYA, Y. & TSURUTA, H. 1991 Experiments on vortex shedding from flat plates with square leading and trailing edges. *J. Fluid Mech.* **222**, 437–447.

NAUDASCHER, E. & ROCKWELL, D. 1994 *Flow-induced vibrations: An Engineering Guide*. A. A. Balkema.

NAUDASCHER, E. & WANG, Y. 1993 Flow-induced vibration of prismatic bodies and grids of prisms. *J. Fluids Struct.* **7**, 341–373.

ONGOREN, A. & ROCKWELL, D. 1988 Flow structure from an oscillating cylinder. Part 1. Mechanisms of phase shift and recovery in the near wake. *J. Fluid Mech.* **191**, 197–223.

PARKER, R. & WELSH, M. C. 1983 Effects of sound on flow separation from blunt flat plates. *Intl J. Heat Fluid Flow* **4**, 113–127.

ROCKWELL, D. & NAUDASCHER, E. 1979 Self-sustained oscillations of impinging free shear layers. *Annu. Rev. Fluid. Mech.* **11**, 67–94.

ROSHKO, A. 1954 On the drag and shedding frequency of two-dimensional bluff bodies. *Tech. Note* 3169. NACA,Washington.

ROSHKO, A. 1995 On the wake and drag of bluff bodies. *J. Aero. Sci.* **124**, 124–132.

SASAKI, K. & KIYA, M. 1991 Three-dimensional vortex structure in a leading-edge separation bubble at moderate Reynolds numbers. *Trans. ASME: J. Fluids Engng* **113**, 405–410.

SHEARD, G. J., THOMPSON, M. C. & HOURIGAN, K. 2003 From spheres to circular cylinders: the stability and flow structures of bluff ring wakes. *J. Fluid Mech.* **492**, 147–180.

SHERWIN, S. J. & KARNIADAKIS, G. EM. 1999 *Spectral/hp Element Methods for CFD*. Oxford University Press.

SIGURDSON, L. W. 1995 The structure and control of a turbulent reattaching flow. *J. Fluid Mech.* **298**, 139–165.

SORIA, J., SHERIDAN, M. & WU, J. 1993 Spatial evolution of the separated shear layer from a square leading-edge plate. *J. Wind Engng Indust. Aero.* **49**, 237–246.

STANSBY, P. K. 1976 Base pressure of oscillating circular cylinders. *J. Engng Mech.* **4**, 591–600.

STAUBLI, T. 1983 Calculation of the vibration of an elastically mounted cylinder using experimental data from forced oscillation. *Trans. ASME: J. Fluids Engng* **105**, 225–229.

STOKES, A. N. & WELSH, M. C. 1986 Flow-resonant sound interaction in a duct containing a plate, II: Square leading edge. *J. Sound Vib.* **104**, 55–73.

TAN, B. T. 2000 Vortex shedding and interaction in flows around bluff plates. PhD thesis, Department of Mechanical Engineering, Monash University.

TAN, B. T., THOMPSON, M. C. & HOURIGAN, K. 1998 Flow around long rectangular plates under cross-flow perturbations. *Intl J. Fluid Dyn.* (http://elecpress.monash.edu.au/IJFD) **2**, Article 1.

THOMPSON, M. C., HOURIGAN, K. & SHERIDAN, J. 1996 Three-dimensional instabilities in the wake of a circular cylinder. *Expl Thermal Fluid Sci.* **12**, 190–196.

WELSH, M. C., HOURIGAN, K., WELCH, L. W., DOWNIE, R. J., THOMPSON, M. C. & STOKES, A. N. 1990 Acoustics and experimental methods: the influence of sound and heat transfer. *Expl Thermal Fluid Sci.* **3**, 138–152.

WILLIAMSON, C. H. K. 1996 Vortex dynamics in the cylinder wake. *Annu. Rev. Fluid Mech.* **28**, 477–526.

WU, J. & SORIA, J. 1992 The character of the instability of the separated shear layer from a square leading edge flat plate. *Proc. 11th Australasian Fluid Mechanics Conf., 14–18 December, Hobart, Australia* (ed. M. R. Davies & G. J. Walker), pp. 391–394.